



Intrapulse Raman scattering and dissipative solitons with extreme spikes

Ivan M. Uzunov¹ · Todor N. Arabadzhiev¹

Received: 10 September 2019 / Accepted: 17 October 2019 / Published online: 2 November 2019
© Springer-Verlag GmbH Germany, part of Springer Nature 2019

Abstract

We have studied numerically the influence of intrapulse Raman scattering (IRS) on the dissipative solitons with extreme spikes (DSES). The following scenarios of the influence of IRS have been identified. In the anomalous dispersion regime, there has been found a transformation of the single spike DSES and pulsating in x and t DSES into Raman dissipative solitons. We should mention a good performance of the finite-dimensional system in the description of all pulse parameters in the first case. In the other scenario, the DSES moving with fixed velocity pulsating in x and t transforms into single spike DSES moving with fixed velocity. We have also observed a transformation of double spike DSES into single spike moving DSES as well as a transformation of a single spike DSES into a single spike moving DSES accompanied by the change in the period of the spikes appearance. In the normal dispersion regime, we have found a transformation of a single spike DSES into a single spike moving DSES and the change of the period of the spikes appearance. For a large strength of IRS, an appearance of a chaotic DSES has been observed.

1 Introduction

The complex cubic–quintic Ginzburg–Landau equation (CCQGLE) has been used to describe many phenomena including second-order phase transitions, superconductivity, superfluidity, Bose–Einstein condensation, liquid crystals, and string theory [1]. In optics, the CCQGLE models passively mode-locked solid-state and fiber lasers as well as soliton transmission lines [2–4]. For ultrashort optical pulses, it is necessary to include some additional higher-order effects (HOE): third-order of dispersion (TOD), self-steepening (SS) and intrapulse Raman scattering (IRS) [5–7]. The formation of fixed-shape solutions from the localized pulsating solutions of the CCQGLE under the influence of HOE has been numerically shown in [5, 6]. In [7], the existence of periodic non-chaotic explosions in the CCQGLE under the influence of IRS has been numerically observed.

Recently, a strongly pulsating regime of dissipative solitons has been numerically observed in the normal and anomalous dispersion regimes [8–10]. The basic feature of the former is extreme ratios of maximal to minimal energies (or amplitudes) in each period of pulsations [8]. In the normal dispersion regime, the solution structure can be considered as sharp peaks developing on top of a more stable wider soliton that serves as a background. Later on, such strongly pulsating dissipative solitons have been named dissipative solitons with extreme spikes (DSESs) [9, 10]. It has been shown that the variation of the parameters of the CCQGLE results in a variety of bifurcations. Bifurcation diagrams have been constructed representing the peak amplitude (or energy) versus any of the parameters of the CCQGLE: dispersion and saturation of the nonlinear gain [8]; linear loss–gain, spectral filtering, nonlinear gain, saturation of the nonlinear gain and saturation of the nonlinear refractive index [9]; and finally, dispersion, spectral filtering and nonlinear gain in [10]. The bifurcation diagrams represent different forms of the DSES [8–10]. The DSES can be either periodic or chaotic. The periodic DSES can be of the following types: single spike pulsating in x (or single spike DSES); double spike pulsating in x (or double spike DSES), moving with fixed velocity single spike pulsating in x (or single spike moving DSES), moving with fixed velocity pulsating in x and t (or asymmetric solution with the profile inverted after every period [10]), and others [8–10].

✉ Todor N. Arabadzhiev
tna@tu-sofia.bg

Ivan M. Uzunov
ivan_uzunov@tu-sofia.bg

¹ Department of Applied Physics, Faculty of Applied Mathematics and Informatics, Technical University of Sofia, 8 Kl. Ohridski Blvd, 1000 Sofia, Bulgaria

Our aim is to study the influence of IRS on DSES. Here, we apply the simplest quasi-instantaneous approximation of the IRS [11, 12]. This can be modeled by the CCQGLE perturbed with Raman term (see Eq. 1 below). The main approach for identifying its solutions is the numerical solution [2, 3, 8–10]. We have numerically solved the CCQGLE using two different numerical approaches: the fourth-order Runge–Kutta in the Interaction Picture (RK4IP) method and the Agrawal split-step method. Our investigation is based on the numerical findings of [8–10] for regions of parameters for which the above-mentioned forms of DSES exist. Although the types of the DSES are very different, some of them like the single spike pulsating in x , centered in t and symmetric in t DSES could be described by the proper finite degrees of freedom model.

Using the method of momentum [13] we have developed the finite degrees of freedom model for the analysis of the influence of HOE on the solutions of the CCQGLE in the anomalous dispersion regime [14]. Here we have applied a finite degree of the freedom model to describe the transformation of a single spike pulsating in x centered in t and symmetric in t DSES into Raman dissipative solitons with large amplitudes. We started to use the model [14] in the study of the influence of IRS, SS, and TOD on some of the solutions of [4]. Using this model, we have predicted and numerically observed by the direct numerical solution of Eq. (1) the appearance of a) a pulsating solution in the presence of SS and IRS as well as b) a pulsating solution in the presence of IRS and large values of nonlinear gain coefficient [15]. Recently, the same dynamical model has helped us to find the existence of Raman limit cycles in the presence of SS, IRS and large nonlinear gain [16].

In the second paragraph, we introduce the CCQGLE perturbed with IRS [see Eq. (1)] as well as the finite degrees of freedom model derived in [14] (Eq. (3)). Next, we discuss the numerical methods as well as the numerical parameters used for the calculation of Eq. (1). The third paragraph contains our results. Finally, we present the conclusions we have drawn from our investigations.

2 Basic equation and dynamical model

The dynamical behavior is described by the following CCQGLE perturbed by IRS [2, 4–7]:

$$i \frac{\partial U}{\partial x} + \frac{D}{2} \frac{\partial^2 U}{\partial t^2} + |U|^2 U = i\delta U + i\beta \frac{\partial^2 U}{\partial t^2} + i\epsilon |U|^2 U - \nu |U|^4 U + i\mu |U|^4 U + \gamma U \frac{\partial}{\partial t} (|U|^2), \tag{1}$$

where U is the normalized envelope of the electric field, t and x are the evolutional and spatial variables, D denotes dispersion, being anomalous when $D > 0$ and normal if $D < 0$, δ is the linear loss–gain coefficient, β describes spectral filtering, ϵ is the nonlinear gain or absorption coefficient (the nonlinear gain arises from saturable absorption), μ , if

negative, accounts for the saturation of the nonlinear gain, ν , if negative, corresponds to the saturation of the nonlinear refraction index. In this equation, we have implied that the group-velocity dispersion is anomalous. The parameter γ is responsible for the effect of IRS in the simplest quasi-instantaneous description. The linear approximation to the frequency-domain Raman response function has been applied in this case [11, 12].

Eq. (1) has been used to model the propagation of optical pulses in soliton transmission systems as well as a master equation in the theory of mode-locked solid-state and fiber lasers [2–4].

We have solved numerically the CCQGLE with the fourth-order Runge–Kutta in the Interaction Picture (RK4IP) method [17] and the Agrawal split-step method with two iterations [18]. The choice of these numerical approaches is related to the results of our recent study [19]. A comparison of the performance of the different numerical methods for the numerical calculation of the influence of the IRS (in the quasi-instantaneous description) on the soliton propagation can be found in [19]. The results presented here are obtained by the step-size adaptive versions of the fourth-order Runge–Kutta in the Interaction Picture (RK4IP) method [17] and the Agrawal split-step method with one and two iterations. As an adaptive step-size selection criterion, we have applied the nonlinear phase increment [20].

We have used the following values of numerical parameters: time window $T = 80$ and number of grid points $N = 32768$. The corresponding temporal resolution and frequency resolution are $\Delta t = 0.00224$ and $\Delta\omega/2\pi = 0.0125$, respectively. In some cases, we also use time window $T = 400$ and number of grid points $N = 524288$. The corresponding temporal resolution and frequency resolution, in this case, are $\Delta t = 0.00076$ and $\Delta\omega/2\pi = 0.0025$, respectively. The step Δx is an adaptive quantity.

The following numerical quantities have been calculated by the numerical solution of Eq. (1): central circular frequency: $\omega_n(x) = \int_{-\infty}^{+\infty} \omega |U(x, \omega)|^2 d\omega / \int_{-\infty}^{+\infty} |U(x, \omega)|^2 d\omega$, peak amplitude: $\eta_n(x) = \max |U(x, t)|, \forall t$, time position: $k_n(x) = \int_{-\infty}^{+\infty} t |U(x, t)|^2 dt / \int_{-\infty}^{+\infty} |U(x, t)|^2 dt$ and width:

$$\sigma_n(x) = \tau(x) / \tau(0), \text{ where } \tau(x) = \int_{-\infty}^{+\infty} |U(x, t)|^2 / \eta_n(x)^2 dt.$$

To study DSES, we have used symmetric and asymmetric initial conditions for the numerical solution of Eq. (1). As is well known, using asymmetric initial conditions can lead to the appearance of moving solutions [10]. Our symmetric initial condition has the form:

$U(0, t) = \eta_0 \operatorname{sech}(t/\sigma_0)$ (including $\sigma_0 = 1/\eta_0$), where η_0 and σ_0 are the initial amplitude and width, respectively. This form of the initial conditions allows us to obtain numerical results comparable to those of the dynamical system (DS) (3). The asymmetric initial conditions are the following: $U(0, t) = \eta_1 \operatorname{sech}((t - k_1)/\sigma_1) + \eta_2 \operatorname{sech}((t - k_2)/\sigma_2)$, where k_1 and k_2 are the initial positions of the pulses.

To derive a finite degrees of freedom model, we have used the following trial function [4, 13]:

$$U(x, t) = \eta(x) \operatorname{sech}\left[\frac{t - k(x)}{\sigma(x)}\right] \exp[i\omega(x)(t - k(x)) + ic(x)(t - k(x))^2], \tag{2}$$

where $\eta(x)$, $\sigma(x)$ and $k(x)$ are, respectively, the amplitude, width and position of the pulse maximum, $\omega(x)$ is the circular frequency, $c(x)$ is the chirp parameter. Applying the method of moments of [13], we have obtained the following dynamical system [14]:

$$\begin{aligned} \frac{d\eta}{dx} &= (\delta - c)\eta + \beta\left(\frac{\eta(-60 - 5\pi^2 + 3\pi^4c^2\sigma^4)}{15\pi^2\sigma^2} - \eta\omega^2\right) + \mu\frac{2}{15}\left(4 + \frac{15}{\pi^2}\right)\eta^5 \\ \frac{d\omega}{dx} &= -4\beta\frac{(1 + \pi^2c^2\sigma^4)\omega}{3\sigma^2} + \frac{8}{15}\gamma\frac{\eta^2}{\sigma^2} \\ \frac{dk}{dx} &= \omega - \frac{2\pi^2}{3}\beta c\omega\sigma^2 \\ \frac{d\sigma}{dx} &= 2c\sigma + \beta\left(\frac{8}{\pi^2\sigma} - \frac{16}{15}\pi^2c^2\sigma^3\right) - \frac{4}{\pi^2}\epsilon\sigma\eta^2 - \frac{4}{\pi^2}\mu\sigma\eta^4 \\ \frac{dc}{dx} &= \left(-2c^2 + \frac{2}{\pi^2\sigma^4} - \frac{2\eta^2}{\pi^2\sigma^2}\right) - \beta\frac{4(3 + \pi^2)c}{3\pi^2\sigma^2} - \nu\frac{32\eta^4}{15\pi^2\sigma^2} \end{aligned} \tag{3}$$

With $\eta_m(x)$, $\omega_m(x)$, $k_m(x)$ and $\sigma_m(x)$, we denote the amplitude, frequency, position and width calculated by the dynamical system (3). These magnitudes will be compared in some of the following figures with the quantities calculated by the numerical solution of Eq. (1): frequency $\omega_n(x)$, peak amplitude $\eta_n(x)$, time position $k_n(x)$, and width $\sigma_n(x)$ as defined above.

The evolution of the DSES into a stationary solution with a sech-like form is crucial for the application of DS (3) in the description of the solution evolution. Obviously only a small part of DSES of Eq. (1) have this type of evolution. As we will see further, DS (3) can be successfully applied for the description of the transformation of a single spike pulsating in x centered in t and symmetric in t DSES into Raman dissipative solitons with large amplitudes.

3 Influence of IRS on DSES

The regions of the parameter space in the CCQGLE where different types of DSES exist have been identified in [8–10]. Our aim here is to study whether under the influence

of the IRS, there appear transformations in the different types of DSES. In addition, we will check the applicability of DS (3) in the description of such phenomena.

We have fixed the following values of the physical parameters: $\delta = -0.1; \beta = 0.3; \mu = -0.001$ [9, 10]. Our study is based on the bifurcation diagrams representing the peak amplitude vs ϵ , for two different values of ν : $\nu = 0.1; \nu = 0.01$ [9, 10]. We should mention that the comparison with the numerical results presented there could have qualitative character (the initial conditions for the numerical calculations are not given in [9, 10]).

First we consider the case of $\nu = 0.01$. As it is well known for $\epsilon = 0.24$, a single spike pulsating in x centered in t and symmetric in t DSES should be expected [9, 10]. We will consider symmetric and asymmetric initial conditions. Here we fix the symmetric initial condition as follows: $U(0, t) = 2.7\operatorname{sech}(3t)$.

As could be expected in this case, we have observed a single spike and symmetric in t DSES [9, 10]. Figure 1a–c, represent the existence of an initial transition period ($x \sim 5$) for the appearance of DSES. A nice preservation of the shape of the DSES symmetric in t , as well as its spectrum at fixed distances can be seen in Fig. 1c, d.

Next in Fig. 2, we have studied what happens to the single spike DSES pulsating in x and symmetric in t in the presence of IRS. We have fixed the value of the parameter describing IRS as: $\gamma = 0.05$.

As we see under the influence of IRS $\gamma = 0.05$ at very short transformation distance $x \sim 1$ from the initial single spike and symmetric in t DSES there appears a stationary solution or a Raman dissipative soliton with an amplitude larger than the minimum but smaller than the maximum peak amplitude of the pulsating solution. The Raman dissipative soliton possesses fixed values of its amplitude, central frequency, and time width. As can be well seen from Fig. 2a, b, these parameters as well as the process of their appearance are very well described by DS (3). An excellent preservation of the time shape and spectrum of the Raman dissipative

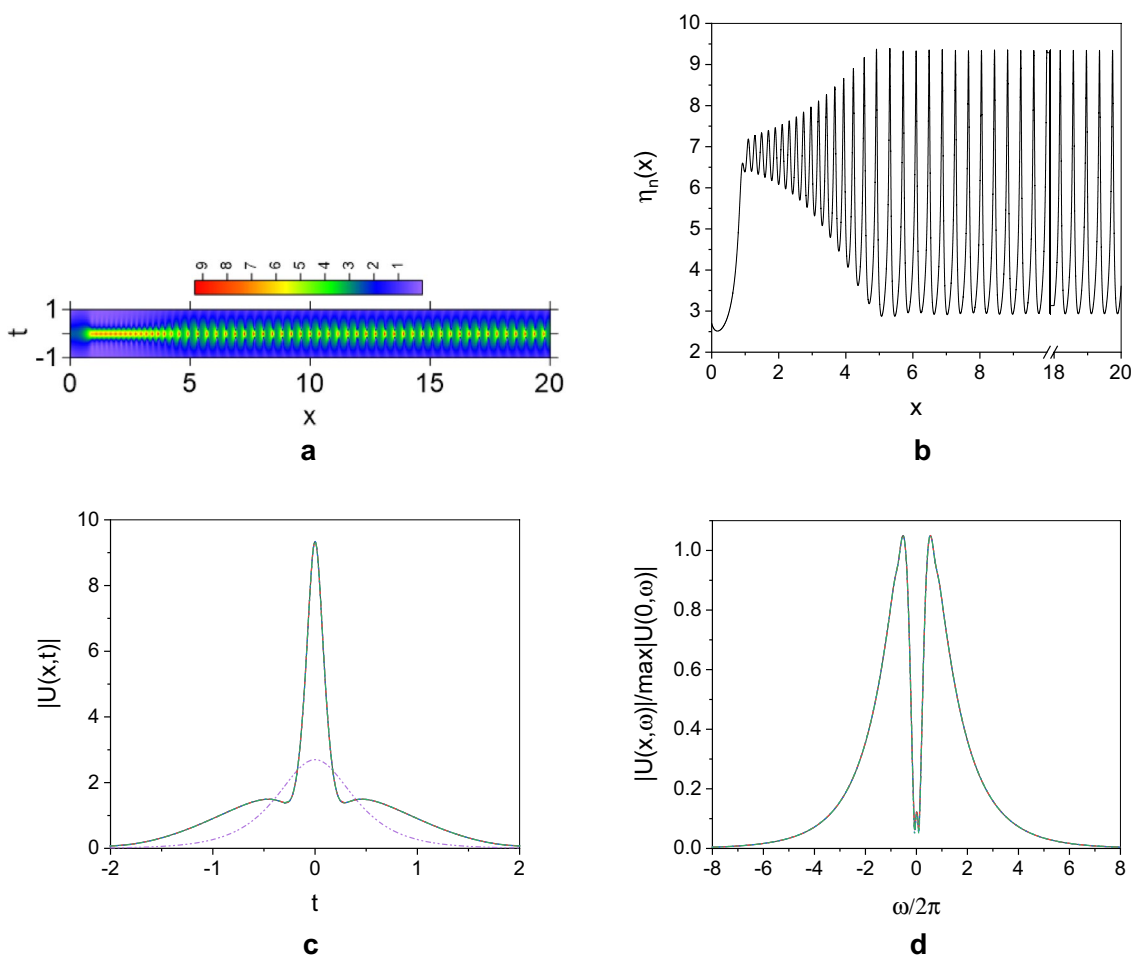


Fig. 1 Results obtained by numerical solution of Eq. (1) with parameters: $\delta = -0.1$; $\beta = 0.3$; $\mu = -0.001$, $\nu = 0.01$; $\varepsilon = 0.24$; $\gamma = 0$ and numerical parameters $N = 32768$; $T = 80$. Initial condition: $U(0, t) = 2.7 \operatorname{sech}(3t)$. **a** Contour plot of the amplitude on the (t, x) plane. **b** Evolution of the peak amplitude of DSES in accordance with

Eq. (1). **c** Comparison of the shapes of DSES at $x = 0$ (dash-dot-dot line) and $x = 8.05; 10; 18.19; 19.74$ (with different colors and lines but they practically coincide). **d** Comparison of the spectrums of the DSES at $x = 8.05; 10; 18.19; 19.74$ (with different colors and lines but they practically coincide)

soliton with respect to distance is observed in Fig. 2c, d, respectively. Figure 2d shows the frequency shift of the central frequency in the spectrum of the numerical solution. The symmetric form of the spectrum should be mentioned also in Fig. 2d. In next Fig. 3, we study the performance of DS(3) in the region of $\gamma \in [0.05 \div 0.09]$ by comparing its results with those obtained from the numerical solution of Eq. (1).

We should mention that there is a good agreement between the results obtained with DS(3) for the amplitudes, positions, frequencies and time widths and those obtained from the numerical solution of Eq. (1).

Keeping all physical and numerical parameters as in Fig. 1, we have applied the asymmetric initial condition: $U(0, t) = 2.7 \operatorname{sech}(3t) + \operatorname{sech}(2t + 3)$. The results for the case without IRS ($\gamma = 0$) are presented in Fig. 4 below.

As can be seen from Fig. 4a, b after some initial transition period, there appears a DSES pulsating in x and t (or

asymmetric solution with the profile inverted after every period [10]) with a maximum value of the amplitude around 9. Comparing Fig. 1a and Fig. 4a, we can conclude that the symmetry of the initial condition is important for the further evolution of the generated DSES. For distances $x = 4.28; 4.67$, there are no oscillations in time; while for the distances $x = 19.56; 19.93$, such oscillations exist. Figure 4c shows the shape of the DSES oscillating in time. Figure 4d shows a preservation of the spectrum of the DSES in the propagation in x can be seen.

In Fig. 5, we have shown how the presence of IRS ($\gamma = 0.05$) changes the DSES pulsating in x and t but not centered in t (presented in Fig. 4).

In Fig. 5a, we can see that after some initial transition period, there appears a Raman dissipative soliton with amplitude around 5. The Raman dissipative soliton

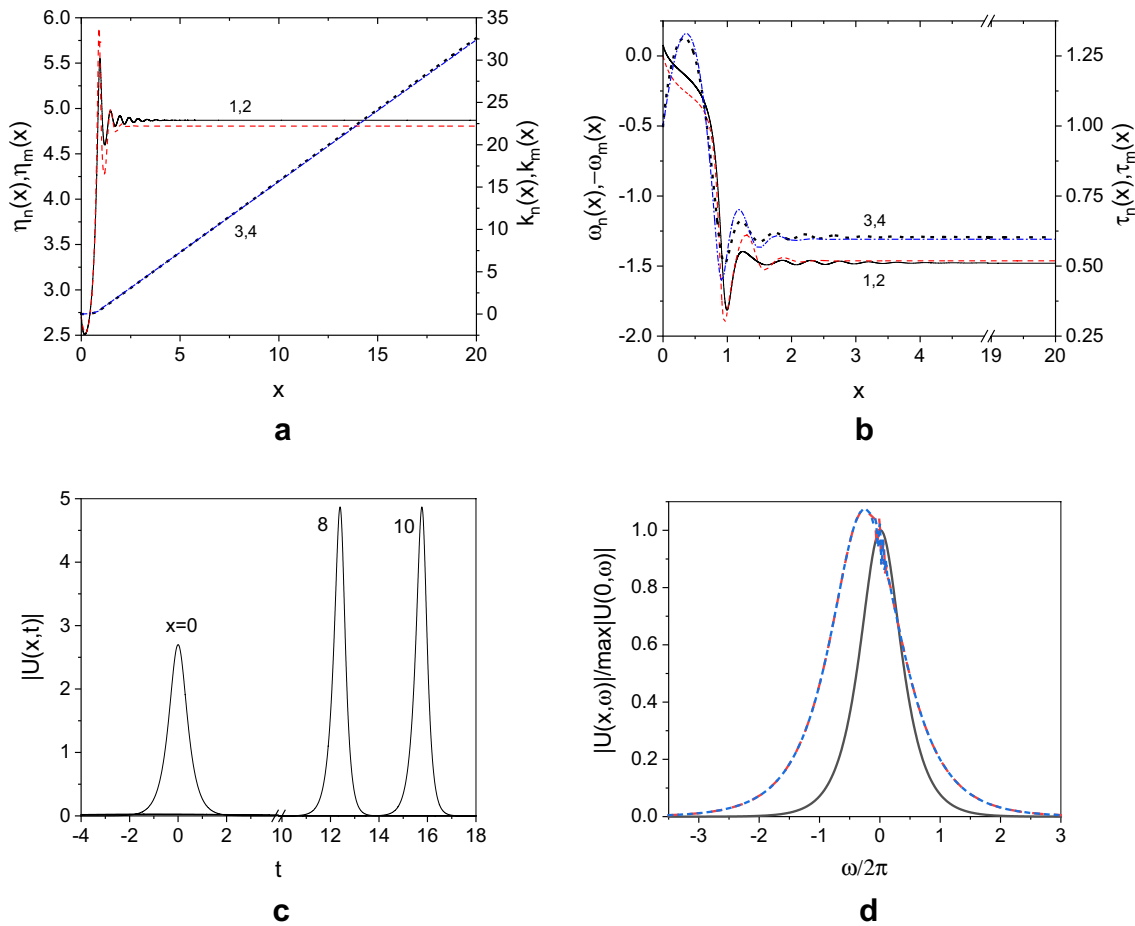


Fig. 2 Results obtained by numerical solution of Eq. (1) and DS (3) with parameters: $\delta = -0.1$; $\beta = 0.3$; $\mu = -0.001$, $\nu = 0.01$; $\varepsilon = 0.24$; $\gamma = 0.05$; numerical parameters: $N = 32768$; $T = 80$. Initial condition: $U(0, t) = 2.7\text{sech}(3t)$. **a** Comparison of the evolutions of solution amplitudes—1,2 and temporal positions—3,4 calculated by Eq. (1) and DS (3). **b** Comparison of the evolutions of central circular frequencies (ω_n and $-\omega_m$)—1, 2 and time widths—3, 4 of solutions calculated by Eq. (1) and DS (3). Notation for **a** and **b**: 1—black solid line, 2—red dash, 3—black dot, 4—blue dash-dot. **c** Comparison of the shapes of DSES at $x = 0; 8; 10$. **d** Comparison of the spectrums of the DSES at $x = 0; 8; 10$ ($x = 0$ —black solid line, $x = 8, 10$ —red dash and blue short-dash lines but they practically coincide)

culated by Eq. (1) and DS (3). Notation for **a** and **b**: 1—black solid line, 2—red dash, 3—black dot, 4—blue dash-dot. **c** Comparison of the shapes of DSES at $x = 0; 8; 10$. **d** Comparison of the spectrums of the DSES at $x = 0; 8; 10$ ($x = 0$ —black solid line, $x = 8, 10$ —red dash and blue short-dash lines but they practically coincide)

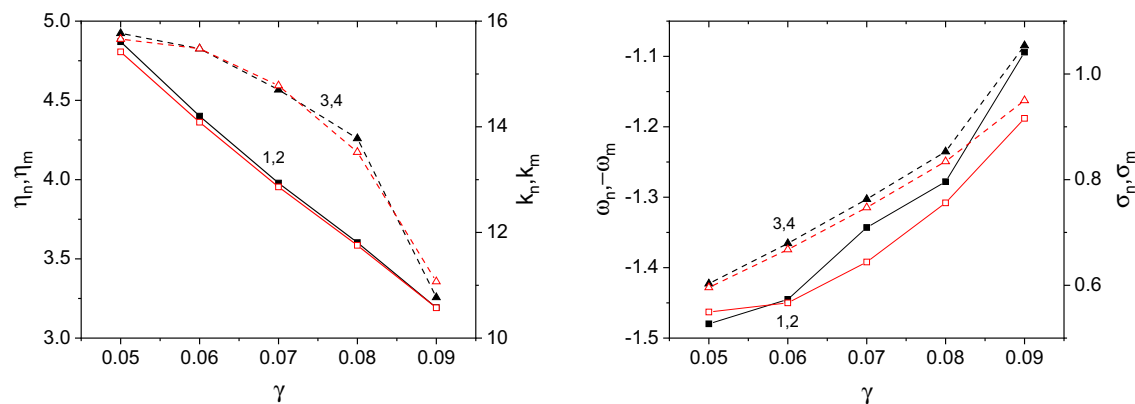


Fig. 3 Results obtained by numerical solution of Eq. (1) and DS (3) at $x = 10$ with parameters: $\delta = -0.1$; $\beta = 0.3$; $\mu = -0.001$, $\nu = 0.01$; $\varepsilon = 0.24$ **a** 1 and 2—numerical and DS peak amplitudes, 3 and 4—numerical and DS positions; **b** 1 and 2—numerical and DS

central circular frequencies (ω_n and $-\omega_m$), 3 and 4—numerical and DS (3) time widths. Notation for **a** and **b** 1—black and 2—red solid lines with squares, 3—black and 4—red dash lines with triangles

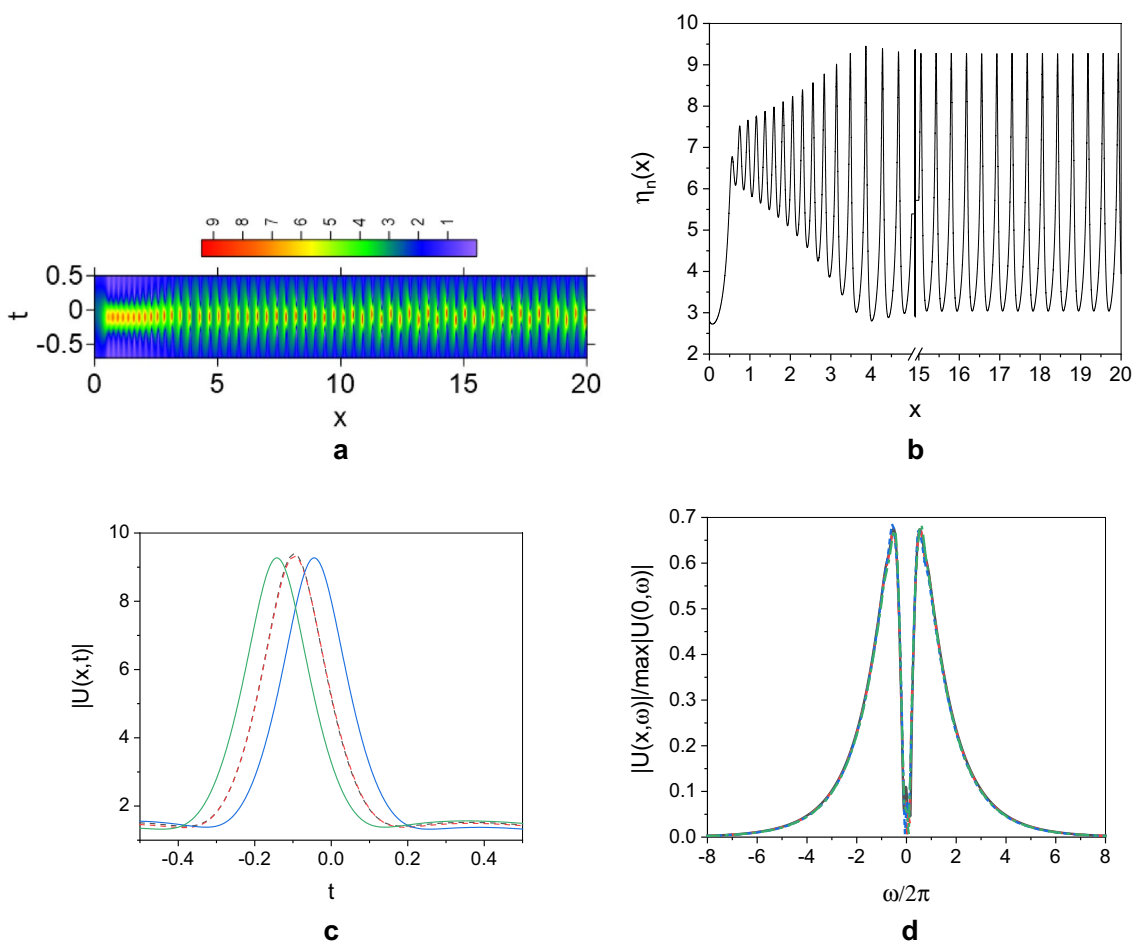


Fig. 4 Results obtained by numerical solution of Eq. (1) with parameters: $\delta = -0.1; \beta = 0.3; \mu = -0.001\delta = -0.1; \beta = 0.08; \nu = 0.01; \epsilon = 0.24; \gamma = 0$ and numerical parameters $N = 32768; T = 80$. Initial condition: $U(0, t) = 2.7\text{sech}(3t) + \text{sech}(2t + 3)$. **a** Contour plot of the amplitude on the (t, x) plane. **b** Evolution of the peak amplitudes of the numerical solution with x . **c** Space evolution of time

shape of DSES at $x = 4.28; 4.67$ —black and red dash lines and $x = 19.56; 19.93$ —blue (left) and green (right) solid lines. **d** Space evolution of the spectrum of DSES at $x = 4.28; 4.67; 19.56; 19.93$ (with different colors and lines but they practically coincide)

possesses fixed values of its amplitude, central frequency, and time width. Comparing Fig. 4 and Fig. 5, we should conclude that in the presence of IRS, pulsating in x and t but not centered in t DSES transforms into Raman dissipative soliton with amplitude smaller than the maximum amplitude and larger than the minimum amplitude of pulsating in x and t DSES. From Fig. 5b, the preservation of the time shape of the dissipative Raman soliton can be seen. No asymmetry in the pulse can be observed. Fig. 5c presents the initial frequency shift toward lower frequency and then the preservation in the position of the spectrum with respect to distance. Specific frequency oscillation should be mentioned just in the center of the frequency domain. There has also been observed a similar influence

of the IRS with $\gamma = 0.05$ on the pulsating in x and t but not centered in t DSES in the case of $\epsilon = 0.25$.

Next, we have looked at what happens with the same asymmetric initial condition: $\psi(0) = 2.7/\cosh(3t) + 1/\cosh(2t + 3)$ for $\epsilon = 0.48$ under the influence of IRS. For $\epsilon \approx 0.48$, a solution with two spikes per period is expected [9, 10]. Figure 6 presents the numerical solution for $\epsilon = 0.48$ without IRS ($\gamma = 0$).

Figure 6a clearly expresses the existence of DSES moving with fixed velocity pulsating in x and t (or asymmetric solution with the profile inverted after every period [10]). Note that from Fig. 6b, this DSES can be considered as a pulsating with two spikes per period solution. The distances that were chosen in Fig. 6c, d are the distances of the

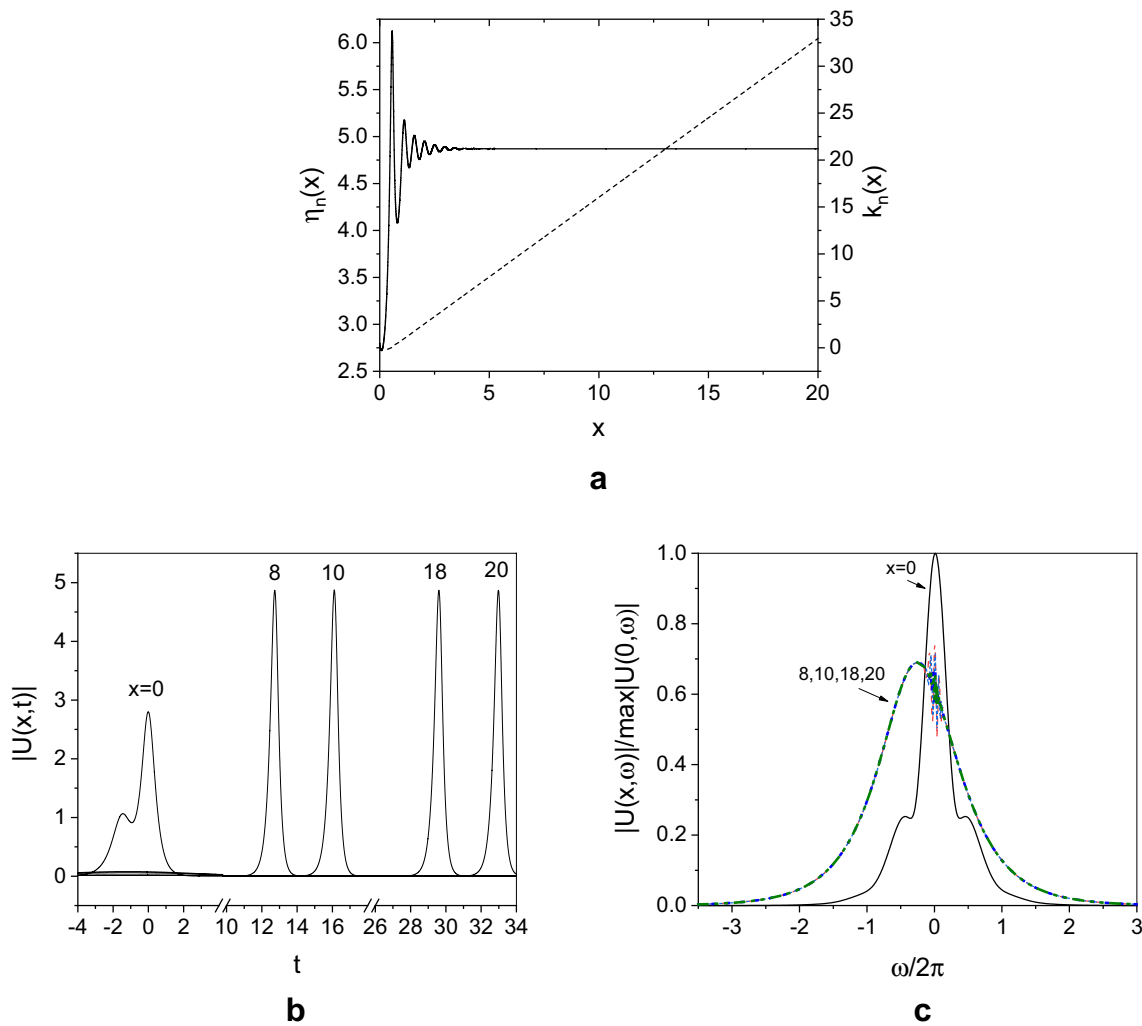


Fig. 5 Results obtained by numerical solution of Eq. (1) with parameters: $\delta = -0.1$; $\beta = 0.3$; $\mu = -0.001$; $\nu = 0.01$; $\epsilon = 0.24$; $\gamma = 0.05$; numerical parameters: $N = 32768$; $T = 80$. Initial condition: $U(0, t) = 2.7\text{sech}(3t) + \text{sech}(2t + 3)$. **a** Spatial evolution of the peak

amplitude (solid line) and temporal position (dash) of the DSES. **b** Space evolution of time shape of DSES at $x = 0; 8; 10; 18; 20$. **c** Space evolution of the spectrum of DSES at $x = 0; 8; 10; 18; 20$

last four spikes in the propagation of the DSES. Figure 6c demonstrates the DSES pulsating in t . Figure 6d presents the corresponding pulsation in the spectrum of the DSES. In Fig. 6c, d we can also see that during pulsations there exist mirror symmetry in the time domain.

Figure 7 shows how the moving with fixed velocity pulsating in x and t DSES from Fig. 6, in the presence of IRS ($\gamma = 0.05$) transforms into a moving with fixed velocity single spike DSES.

As can be seen from Fig. 7a, the moving with fixed velocity pulsating in x and t DSES from Fig. 6 under the influence of IRS transforms into moving with fixed velocity single spike pulsating in x DSES. Figure 7b clearly shows the appearance of a single spike solution. The distances that

were chosen in Fig. 7c, d are the distances of the last four spikes in the propagation of the DSES shown in Fig. 7a. The main observation from Fig. 7c is the appearance of asymmetric single spike DSES. Its maximum amplitude reduces to approximately 14. Figure 7c also demonstrates the time shift of the DSES under the influence of the IRS. Finally, Fig. 7d presents the asymmetric form of the spectrum of the moving with fixed velocity single spike DSES.

Next, we consider the case of $\nu = 0.1$. As it is well known for $\epsilon = 0.4$ and $\epsilon = 0.42$, a double spike and a single spike DSES should be expected, respectively [9, 10]. The influence of IRS $\gamma = 0.05$ on these solutions is presented in the Figs. 8 and 9. Below you can see first the case of $\epsilon = 0.4$.

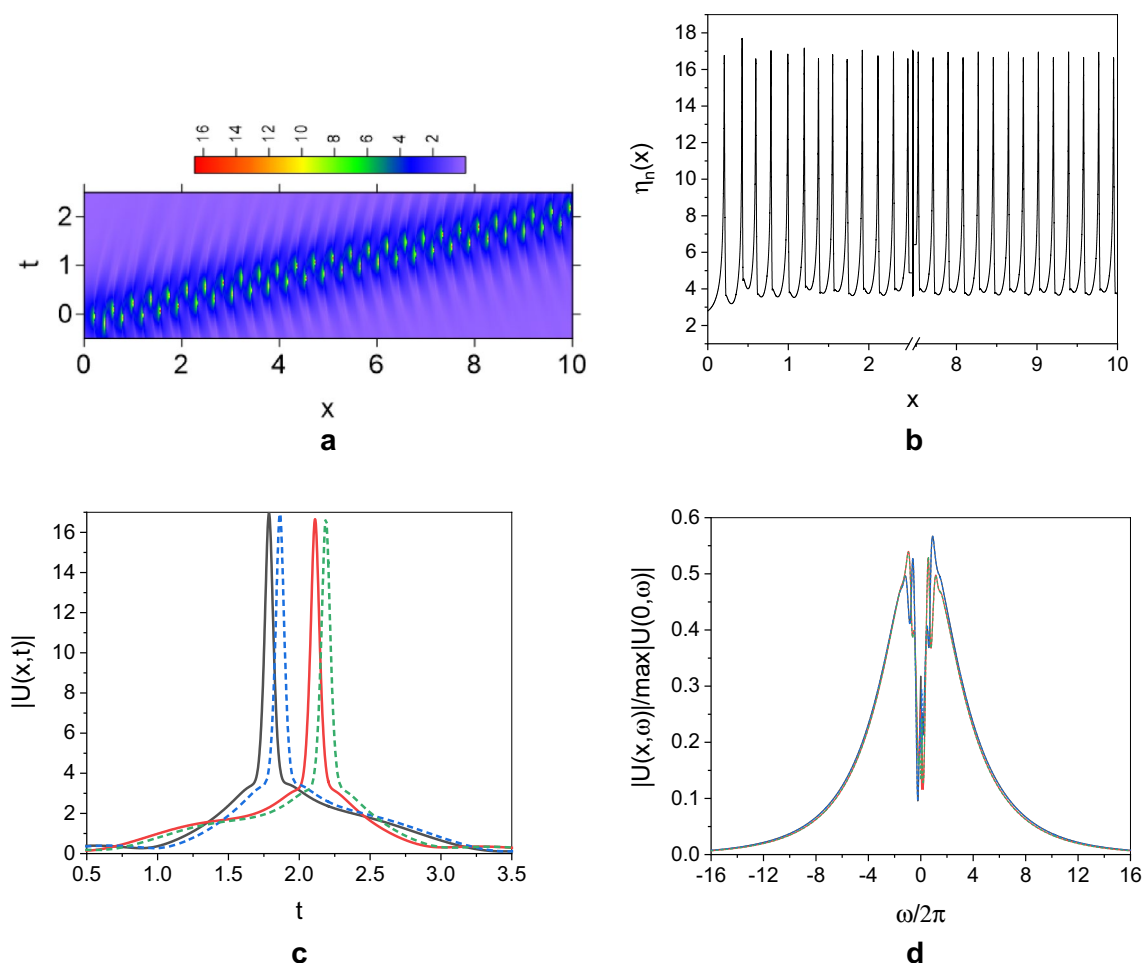


Fig. 6 Results obtained by numerical solution of Eq. (1) with parameters: $\delta = -0.1$; $\beta = 0.3$; $\mu = -0.001$; $\nu = 0.01$; $\varepsilon = 0.48$; $\gamma = 0$ and numerical parameters $N = 32768$; $T = 80$. Initial condition: $U(0, t) = 2.7\text{sech}(3t) + \text{sech}(2t + 3)$. **a** Contour plot of the amplitude on the (t, x) plane. **b** Evolution of the peak amplitude of the numerical

solution. **c** Spatial evolution of the time shape of four consecutive DSES at $x = 9.39; 9.58$ (black and red solid line) and $x = 9.77; 9.95$ (blue and green dash lines). **d** The spectrum of these DSES ($x = 9.39; 9.58; 9.77; 9.95$)

As expected, a pulsating in x double spike DSES is observed in Fig. 8a, c. Figure 8c shows the transformation of the double spike DSES into a single spike moving DSES. The spike profiles in Fig. 8a, b and all the other 3D-space profile figures are arranged in a formation of the spikes along the x -axis which shows the distance of the formation. The main observation from Fig. 8b is the appearance of asymmetric single spike DSES pulsating in x . Its maximum amplitude is smaller than the amplitude of the largest initial double spike (Fig. 8c). The corresponding time shift due to IRS is observed in Fig. 8b. Under the influence of IRS there appear changes in the distance between the spikes. There follows the case of $\varepsilon = 0.42$.

As expected, a single spike DSES is observed in Fig. 9a, c (in black). In Fig. 9b, c (in red), we observe a transformation of a single spike DSES into a single spike DSES moving with constant velocity under the influence of IRS. However, as can be seen from Fig. 9b to Fig. 9d, the DSES moving with constant velocity has an asymmetric shape in time. This asymmetric time shape of the moving DSES is preserved very well with the distance. Despite the asymmetry of the shape of DSES, its central part can be well approximated with the symmetric function whose maximum amplitude and full-width at half-maximum (FWHM) time width are not affected by distance. The corresponding time shift due to IRS is well observed in Fig. 9b, d. Figure 9c shows a reduction in the amplitudes. The change between distances at

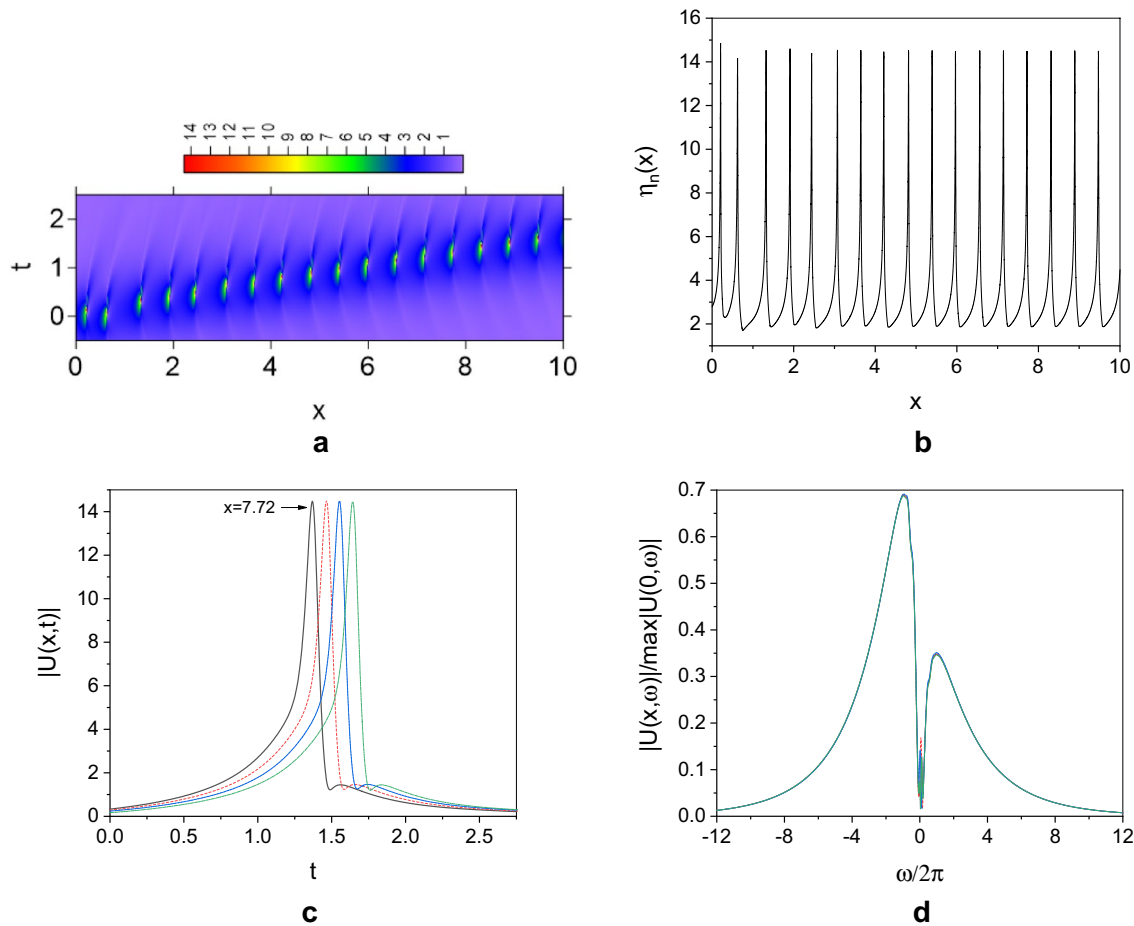


Fig. 7 Results obtained by numerical solution of Eq. (1) with parameters: $\delta = -0.1; \beta = 0.3; \mu = -0.001; \nu = 0.01; \epsilon = 0.48; \gamma = 0.05$ and numerical parameters $N = 32768; T = 80$. Initial condition: $U(0, t) = 2.7\text{sech}(3t) + \text{sech}(2t + 3)$. **a** Contour plot of the amplitude on the (t, x) plane. **b** Spatial evolution of the peak ampli-

tude of the DSES. **c** Space evolution of time shape of DSES at $x = 7.72; 8.81; 8.89; 9.47$ (black solid, red dash, blue solid, green dash-dot lines). **d** The spectrum of the same DSES at $x = 7.72; 8.81; 8.89; 9.47$ (the spectrums practically coincide)

which successive spikes appear under the influence of IRS is demonstrated in Fig. 9e. Clearly, the distance between the single spikes increases under the influence of IRS.

Finally, we present some examples of the influence of IRS on DSES in the normal dispersion regime. In Fig. 10, we study the case of large $\epsilon = 0.95$ with which demonstrates the existence of a single spike DSES [8].

Figure 10a, b, in the absence of the IRS, shows the existence of a single spike pulsating in x DSES [8]. In the presence of IRS after an initial transition distance (~ 4 , increases with γ) there appears a moving single spike pulsating in x DSES that propagates practically with full preservation of its shape in time regardless of the large value of the parameter describing IRS. This is quite an interesting robustness of the time shape of the moving single spike pulsating in

x DSES in the presence of IRS. It can clearly be seen in Fig. 10a that under the influence of IRS there appears well-expressed time shift of the DSES to the left. As expected, in Fig. 8 and Fig. 9 due to the influence of IRS, the distance in x between the single spikes increases. In the case of $\gamma = 0$, the distance between single spikes is $\delta x \approx 0.28$; while for $\gamma = 0.15$ and $\gamma = 0.3$, it is $\delta x \approx 0.32$ and $\delta x \approx 0.6$. A similar type of behavior is observed in the case of $\gamma = 0.15$. The important conclusion which can be drawn from these results is that for $\nu = 0.1$ and $\epsilon = 0.95$ even in the presence of a strong IRS influence (values of $\gamma = 0.15; 0.3$), the generated moving single spike DSES demonstrates full preservation of its shape. In Fig. 10c, we can first see the typical spectrum shape of the DSES in the normal dispersion regime found in [8] as well as its preservation during its propagation. In the

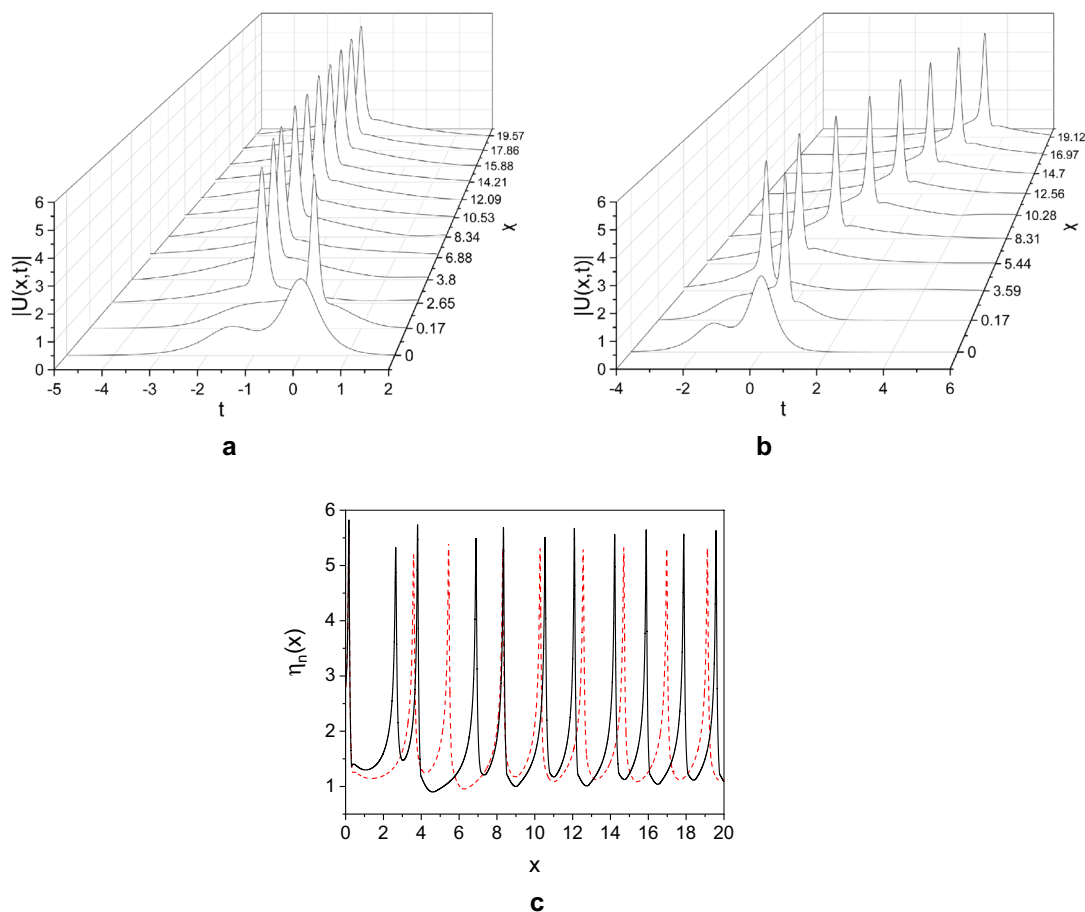


Fig. 8 Results obtained by numerical solution of Eq. (1) with parameters: $\delta = -0.1; \beta = 0.3; \nu = 0.1; \mu = -0.001$. The numerical parameters are: $N = 32768; T = 80$. Initial condition: $U(0, t) = 2.7\text{sech}(3t) + \text{sech}(2t + 3)$. Space evolution of time shape of DSES for cases **a** $\epsilon = 0.4; \gamma = 0$ and **b** $\epsilon = 0.4; \gamma = 0.05$. The

spike profiles in these 3D-space profile figures are arranged in the order of formation of the spikes along the x axis—where the distance of formation is shown. **c** Peak amplitude of DSES as function of x for: **a** (black solid line) and **b** (red dash)

presence of IRS, this spectrum becomes slightly asymmetric and on its left side, the value of the maximum lobe amplitudes increases. There can also be seen a full preservation of the modified spectrum of the DSES with distance.

The results for a larger IRS coefficient value $\gamma = 0.5$ are presented in the Fig. 11.

Figure 11a, b shows that under the strong influence of the IRS, the generated single spike moving DSES starts chaotically to change its positions and later, its form. A similar behavior has been observed at a shorter distance (before the disappearing of DSES) and for $\gamma = 0.75$. The important conclusion here is that there may appear chaotic behavior of DSES under the influence of IRS.

4 Conclusions

We have studied numerically the influence of intrapulse Raman scattering (IRS) on the dissipative solitons with extreme spikes (DSES). We have solved numerically CCQGLE perturbed with IRS using the fourth-order Runge–Kutta in the Interaction Picture (RK4IP) method [17] and the Agrawal split-step method with two iterations [18]. As adaptive step-size selection criteria, we have applied the nonlinear phase increment [20]. There has been found a very good agreement between the results obtained by these two methods. There has also been applied a finite degrees of freedom model for the analysis of the influence of IRS on the solutions of the CCQGLE proposed in [14].

There has been found the following scenarios of the influence of IRS in the anomalous dispersion regime. In

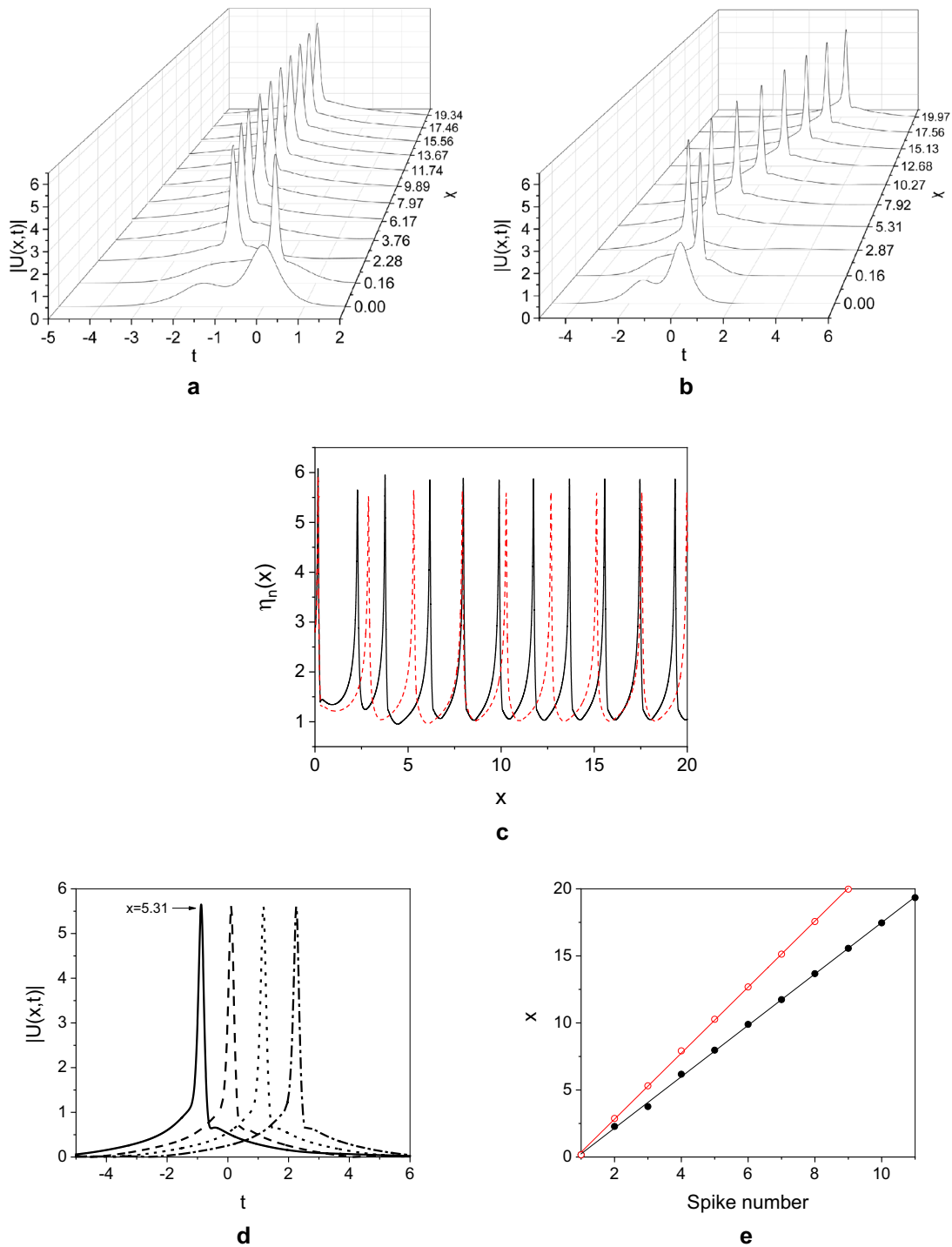


Fig. 9 Results obtained by numerical solution of Eq. (1) with parameters: $\delta = -0.1; \beta = 0.3; \nu = 0.1; \mu = -0.001$. The numerical parameters are: $N = 32768; T = 80$. Initial condition: $U(0, t) = 2.7\text{sech}(3t) + \text{sech}(2t + 3)$. **a** Space evolution of time shape of DSES for $\epsilon = 0.42; \gamma = 0$; **b** Space evolution of time shape of DSES for $\epsilon = 0.42; \gamma = 0.05$. **c** Spatial evolution of peak amplitude of DSES

as function of x for: **a** and **b**. **d** Time shape of DSES at distances: $x = 5.31; 10.27; 15.24; 19.67$ (solid, dash, dot, dash-dot lines). **e** The formation distance for each spike in the sequence presented in **a** without (with black solid circles) and with IRS $\gamma = 0.05$ (with red empty circles). The lines are built by the linear regression and had slopes correspondingly 1.9161 for the case without IRS and 2.4616 with IRS

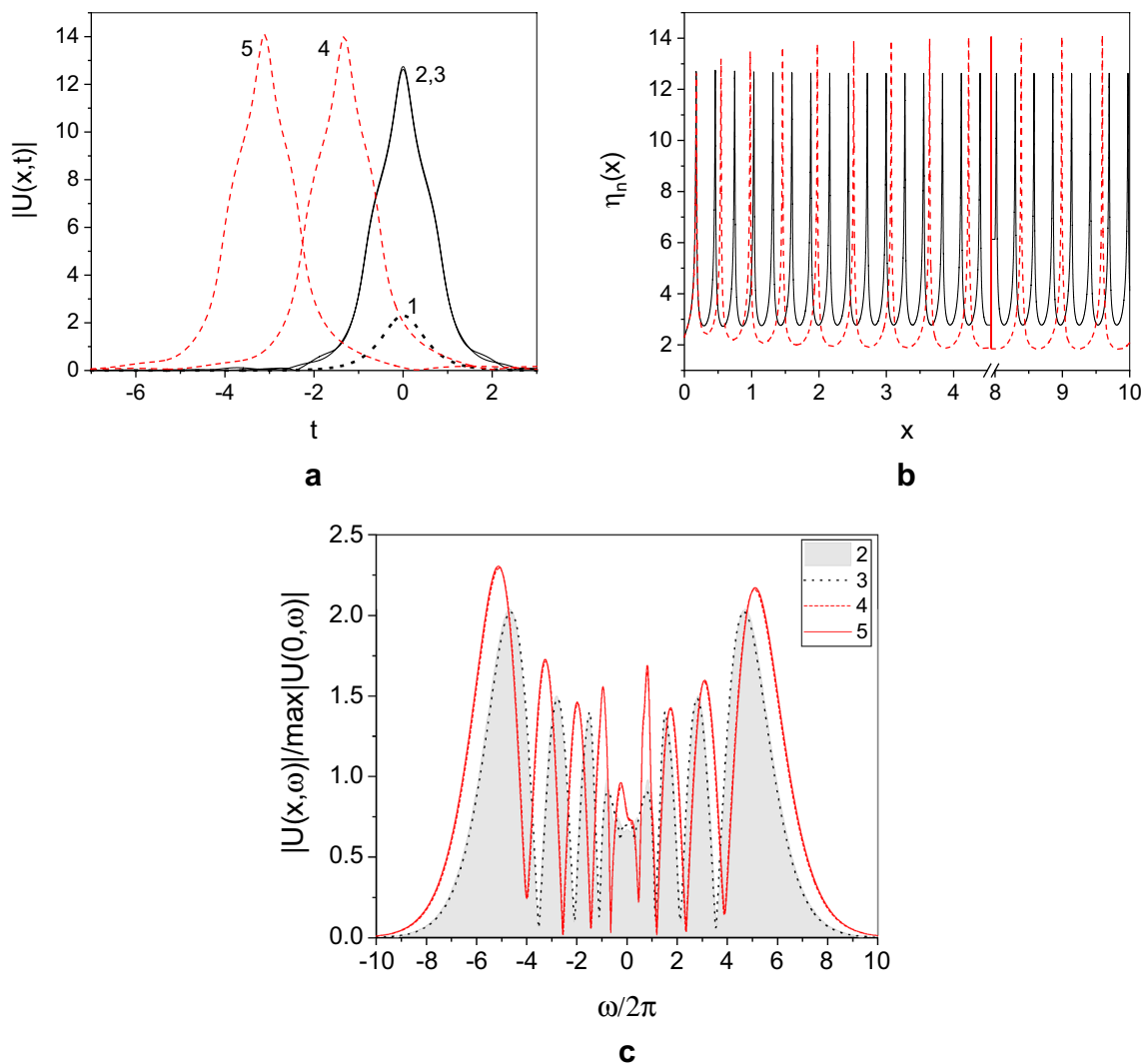


Fig. 10 Results obtained by numerical solution of Eq. (1) with parameters: $\delta = -0.1; \beta = 0.125; \epsilon = 0.95; \nu = 0.1; \mu = -0.001$ (these parameters have been used in [8]) and numerical parameters $N = 32768; T = 80$. Initial condition: $U(0, t) = 2.3 \operatorname{sech}(2.3t)$. **a** Space evolution of time shape of DSES for the two cases: First case (in black)— $\gamma = 0$ where 1 is the initial shape (dots), 2 and 3 (solid lines)

are shapes at $x = 0.45$ and $x = 9.97$ (this case is presented in [8]). The second case (in red)— $\gamma = 0.3$, where 4 and 5 are shapes of the moving DSES at $x = 4.22$ and $x = 9.59$ (dash). **b** Space evolution of the peak amplitude of DSES in case $\gamma = 0$ (black solid line) and $\gamma = 0.3$ (red dash). **c** The spectrum of the DSES for 2–3 (gray full area, black dots), 4–5 (red dash, solid)

the case of $\nu = 0.01$ and nonlinear gain ($\epsilon = 0.24 \div 0.25$), we have found a transformation of single spike DSES and pulsating in x and t DSES into Raman dissipative solitons. A good performance of the finite-dimensional system in the description of all pulse parameters in the first case should be mentioned. In the other scenario with $\epsilon = 0.48$, the moving with fixed velocity pulsating in x and t DSES transforms into a moving with fixed velocity single spike DSES. In the case of $\nu = 0.1$ for nonlinear gain $\epsilon = 0.40$, we have observed a transformation of a double spike DSES into a single spike moving DSES. For $\epsilon = 0.42$, the single

spike DSES transforms into a single spike moving DSES accompanied by conservation of the peak amplitude and the FWHM time width as well as a change in the period of spikes appearance in x . In the normal dispersion regime for large values of nonlinear gain ($\epsilon = 0.95$), we have found a transformation of a single spike DSES into a single spike moving DSES. We have also observed a change of the period of the spikes appearance for IRS $\gamma \leq 0.3$ and appearance of chaotic DSES for IRS $\gamma \geq 0.5$.

We believe that the different scenarios of the influence of IRS on the DSES could be practically important in the study of DSES in laser systems.

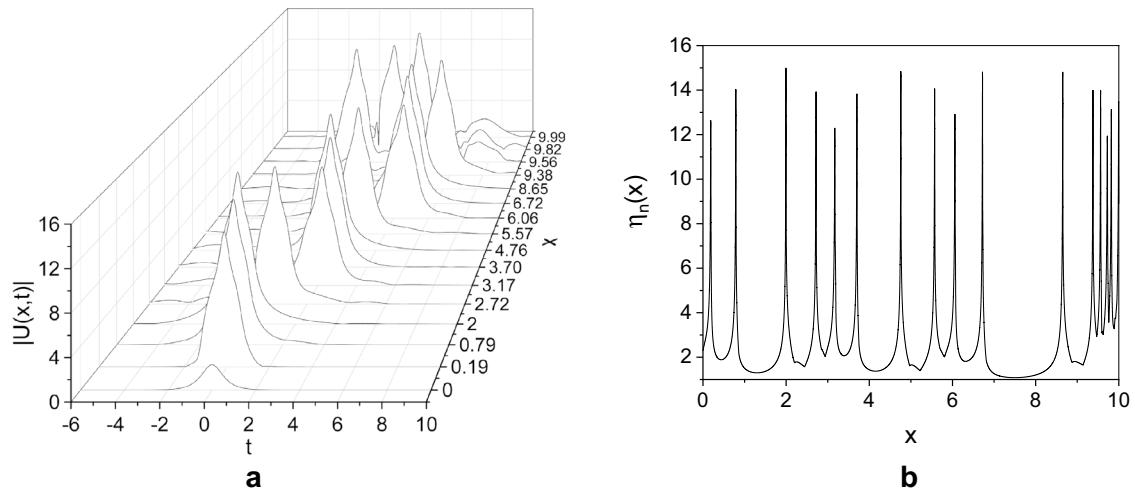


Fig. 11 Results obtained by numerical solution of Eq. (1) with parameters: $\delta = -0.1$; $\beta = 0.125$; $\varepsilon = 0.95$; $\nu = 0.1$; $\mu = -0.001$ $\gamma = 0.5$ and numerical parameters $N = 32768$; $T = 80$. Initial condition:

$U(0, t) = 2.3 \operatorname{sech}(2.3t)$. **a** Space evolution of time shape of DSES on the (t, x) plane. **b** Evolution of the peak amplitude of the numerical solution

References

- M.C. Cross, P.C. Hohenberg, *Rev. Mod. Phys.* **65**, 854 (1993)
- N.N. Akhmediev, J.M. Soto-Crespo, G. Town, *Phys. Rev. E* **63**, 056602 (2001)
- N.N. Akhmediev, A. Ankiewicz, in *Dissipative solitons*, ed. by N.N. Akhmediev, A. Ankiewicz (Springer, Berlin, 2005)
- E. Tsoy, A. Ankiewicz, N.N. Akhmediev, *Phys. Rev. E* **73**, 036621 (2006)
- L. Song, L. Li, Z. Li, G. Zhou, *Opt. Commun.* **249**, 301 (2005)
- S.C. Latas, M.F.S. Ferreira, M. Facao, *Appl. Phys. B* **104**, 131 (2011)
- C. Cartes, O. Descalzi, *Fiber Integr. Opt.* **34**, 14 (2015)
- W. Chang, J.M. Soto-Crespo, P. Vouzas, N.N. Akhmediev, *Phys. Rev. E* **92**, 022926 (2015)
- J.M. Soto-Crespo, N. Devine, N.N. Akhmediev, *JOSA B* **34**, 1542 (2017)
- N.N. Akhmediev, J.M. Soto-Crespo, P. Vouzas, N. Devine, W. Chang, *Phil. Trans. R. Soc. A* **376**, 20180023 (2018)
- R.H. Stolen, J.P. Gordon, W.J. Tomlinson, H.A. Haus, *JOSA B* **6**, 1159–1166 (1989)
- M. Erkinalo, G. Genty, B. Wetzel, J.M. Dudley, *Opt. Express* **18**, 25449–25460 (2010)
- A.I. Maimistov, *J. Exp. Theor. Phys.* **77**, 727 (1993)
- I.M. Uzunov, T.N. Arabadzhiev, *ZhD Georgiev, Opt. Fiber Technol.* **24**, 15 (2015)
- I.M. Uzunov, *ZhD Georgiev, T.N. Arabadzhiev, Phys. Rev. E* **97**, 052215 (2018)
- I. M. Uzunov, T. N. Arabadzhiev, *Zh. D. Georgiev. AIP Conference Proceedings*, vol. 2075, no.1 (AIP Publishing, Melville, 2019)
- J. Hult, *J. Lightwave Technol.* **25**, 3770–3775 (2007)
- M.J. Potasek, G.P. Agrawal, S.C. Pinault, *J. Opt. Soc. Am. B* **3**, 205–211 (1986)
- I.M. Uzunov, T.N. Arabadzhiev, *Opt. Quantum Electr.* **51**(8), 283 (2019)
- O.V. Sinkin, R. Holzlohner, J. Zweck, C.R. Menyuk, *J. Lightwave Technol.* **21**, 61–68 (2003)

Publisher's Note Springer Nature remains neutral with regard to jurisdictional claims in published maps and institutional affiliations.